

# Structure and rheology of suspensions of spherical strain-hardening capsules

Othmane Aouane<sup>1†</sup>, Andrea Scagliarini<sup>2,3</sup> and Jens Harting<sup>1,4</sup>

<sup>1</sup>Helmholtz Institute Erlangen-Nürnberg for Renewable Energy, Forschungszentrum Jülich, Fürther Straße 248, 90429 Nürnberg, Germany

<sup>2</sup>Istituto per le Applicazioni del Calcolo 'M. Picone', IAC-CNR, Via dei Taurini 19, 00185 Roma, Italy

<sup>3</sup>INFN, sezione Roma "Tor Vergata", via della Ricerca Scientifica 1, 00133 Roma, Italy

<sup>4</sup>Department of Chemical and Biological Engineering and Department of Physics, Friedrich-Alexander-Universität Erlangen-Nürnberg, Fürther Straße 248, 90429 Nürnberg, Germany

(Received xx; revised xx; accepted xx)

We investigate the rheology of strain-hardening spherical capsules, from the dilute to the concentrated regime under a confined shear flow using three-dimensional numerical simulations. We consider the effect of capillary number, volume fraction and membrane inextensibility on the particle deformation and on the effective suspension viscosity and normal stress differences of the suspension. The suspension displays a shear-thinning behaviour which is a characteristic of soft particles such as emulsion droplets, vesicles, strain-softening capsules, and red blood cells. We find that the membrane inextensibility plays a significant role on the rheology and can almost suppress the shear-thinning. For concentrated suspensions a non-monotonic dependence of the normal stress differences on the membrane inextensibility is observed, reflecting a similar behaviour in the particle shape. The effective suspension viscosity, instead, grows and eventually saturates, for very large inextensibilities, approaching the solid particle limit. In essence, our results reveal that strain-hardening capsules share rheological features with both soft and solid particles depending on the ratio of the area dilatation to shear elastic modulus. Furthermore, the suspension viscosity exhibits a universal behaviour for the parameter space defined by the capillary number and the membrane inextensibility, when introducing the particle geometrical changes at the steady-state in the definition of the volume fraction.

**Key words:** Capsules, suspensions, rheology

## 1. Introduction

Capsules are closed elastic polymeric membranes, formed by cross-linking proteins to polysaccharides, and encapsulating a liquid droplet core (Lévy & Edwards-Lévy 1996; Häner *et al.* 2020). Their typical diameter spans from a few nanometres to a few millimetres. Capsules are primarily used as controlled delivery systems of active substances with practical applications gearing around pharmaceutical industry (Donbrow 1991; De Cock *et al.* 2010), food processing (Sagis *et al.* 2008), cosmetics (Miyazawa *et al.* 2000), and household products such as paints (Suryanarayana *et al.* 2008). The release

---

† Email address for correspondence: o.aouane@fz-juelich.de

mechanisms of the active agents cover time scales going from a few seconds to days and can occur either via capsule burst or through slow and prolonged diffusion (Neubauer *et al.* 2014). Capsules can exhibit a strain-softening or a strain-hardening behaviour when subject to external stresses depending on the composition of their membrane. Those behaviours can be well recovered with hyperelastic constitutive laws such as Mooney-Rivlin, Neo-Hookean, and Skalak laws (Barthès-Biesel 2016). Strain-softening capsules will burst under continuous elongation (Li *et al.* 1988; Walter *et al.* 2001), similar to droplets, while strain-hardening capsules can sustain very large deformations without membrane rupture (Barthès-Biesel *et al.* 2002; Dodson III & Dimitrakopoulos 2008) making them a good model for mimicking biological cells.

Most practical applications of capsules involve many particle interactions, and often different coupled time scales, with non-linearity appearing already on the level of the single particle mechanics. This level of complexity requires a numerical approach to understand the behaviour of suspensions of capsules, the correlation between their microstructure and rheology, and how it compares with well studied systems such as solid particles and emulsions of drops.

The rheology of a dilute suspension of rigid spheres in an unbounded shear flow has been addressed analytically in the original work of Einstein (1906, 1911) and extended to the second order by Batchelor & Green (1972) to include pair hydrodynamic interactions. Empirical, semi-empirical, and analytical models were proposed in the literature to predict the change of the relative viscosity with the volume fraction of rigid sphere suspensions from the dilute to the concentrated regimes (Eilers 1941; Mooney 1951; Maron & Pierce 1956; Krieger & Dougherty 1959; Frankel & Acrivos 1967). Experiments and numerical simulations have revealed that a suspension of rigid particles exhibits shear-thinning, Newtonian, and shear-thickening behaviour, respectively, as the shear rate is increased. Both normal stress differences,  $N_1$  and  $N_2$ , have been reported to bear a negative sign with a larger magnitude for  $N_2$  with respect to  $N_1$ . The sign of  $N_1$  is still subject to discussions because its magnitude is very small. Numerical simulations performed by Sierou & Brady (2002) and Gallier *et al.* (2014, 2016) have pointed toward the possibility of two distinct physical origins of both normal stress differences.  $N_2$  is associated to particle-particle collisions, while  $N_1$  is mostly of hydrodynamic nature and is significantly affected by the presence or absence of boundaries. Detailed reviews on the rheology of solid particle suspensions can be found in Stickel & Powell (2005), Mueller *et al.* (2010), and Guazzelli & Pouliquen (2018).

Non-Newtonian behaviour in the form of shear-thinning has been reported for emulsions of drops, strain-softening capsules, and closed phospholipid bilayer membranes (vesicles). These three classes of deformable particles are characterized by a thin, continuous, and impermeable interface encapsulating an internal fluid. However, the interface mechanical properties are different. They all exhibit a negative  $N_2$  and a positive  $N_1$ , and unlike rigid particles, the magnitude of  $N_1$  is larger than  $N_2$  which most probably indicates a more dominant role of hydrodynamic interactions as compared to particle-particle collisions (Loewenberg & Hinch 1996; Clausen *et al.* 2011; Matsunaga *et al.* 2016; Vlahovska & Gracia 2007; Zhao & Shaqfeh 2013; Kaoui *et al.* 2014). In analogy to drops, a capillary number, quantifying the shear elastic resistance of the membrane to external stresses, has been widely used in the literature of capsules regardless of the nature of the hyperelastic law and the number of moduli characterizing the membrane mechanics. Bagchi & Kalluri (2010) have shown that for a single strain-hardening capsule under a simple shear flow, the ratio of the area dilatation to shear elastic moduli, characterising the local inextensibility of the membrane, leads to some atypical effects on the intrinsic viscosity and the shear-thinning behaviour. For a non-dilute suspension of anisotropic

strain-hardening capsules, Gross *et al.* (2014) have reported that for small capillary number the impact of the ratio of the area dilatation to shear elastic moduli on the suspension rheology is negligible. To the best of our knowledge the contribution of the local inextensibility of the membrane to the rheology of semi-dilute and concentrated suspensions of initially spherical strain-hardening capsules has so far not been studied. Unfortunately, this field is also lacking experimental data on semi-dilute and concentrated suspensions of capsules despite showing promising applications and future perspectives in areas such as thermal energy storage (Sarı *et al.* (2010)), and injectable scaffolds for soft tissue regeneration (Munarin *et al.* 2010).

This paper is devoted to the study of a specific class of soft particles, capsules with strain-hardening properties which are traditionally used as a mathematical model for simulating blood cells (Freund (2013); Sinha & Graham (2015)). The purpose here is not to draw an analogy to blood, but rather to understand the key parameters governing the rheological properties of an understudied system in the non-dilute regime while comparing its behaviour with well-studied systems such as rigid spheres and emulsions, and hopefully help to tailor possible experiments or applications based on our results. Our second aim is to investigate the peculiar effects observed by Bagchi & Kalluri (2010) and extend those results to the concentrated limit.

We consider a suspension of initially spherical strain-hardening capsules subject to a confined shear flow in the low particle Reynolds number limit. The fluids inside and outside the capsules are Newtonian and considered to have the same densities and viscosities. Under those conditions the capsules can only undergo a tank-treading motion. We use the Skalak 2D hyperelastic constitutive law (Skalak *et al.* (1973)) which provides the capsule membrane with resistances to shear elasticity and local area dilatation. Our study covers a range of volume fractions going from 0.001 to 0.5 and capillary numbers from 0.1 to 1. The shape of the capsules is then a function of the capillary number, the volume fraction, and the membrane local inextensibility. The mean deformation and orientation of the capsules as well as the relative viscosity and normal stress differences are investigated. We use a D3Q19 lattice Boltzmann method (LBM) combined with the immersed boundary method (IBM) and the finite element method (FEM) as described in Krüger *et al.* (2011); Krüger *et al.* (2013, 2014).

The remainder of the paper is organised as follows: We describe the numerical method and the accuracy of the measured quantities in § 2. We then present and discuss our numerical results for the dilute, semi-dilute and concentrated regimes as a function of the parameter  $C$  quantifying the inextensibility of the membrane and the capillary number  $Ca$  in § 3. The concluding remarks and further discussions are given in § 4.

## 2. Simulation approach

The Navier-Stokes equations are recovered in the limit of small Mach and Knudsen numbers by the LBM, which is based on the discretization of the Boltzmann equation in time and phase space (Benzi *et al.* (1992)). The LBM describes the evolution of the single particle distribution function  $f_i(\mathbf{x}, t)$  at a position  $\mathbf{x}$  and time  $t$  with a microscopic velocity  $\mathbf{c}_i$ , where  $i = 1 \dots Q$ , on a regular  $D$ -dimensional lattice in discrete time steps  $\Delta t$ . We consider in this work a D3Q19 model corresponding to a three-dimensional lattice with  $Q = 19$  velocities. The lattice Boltzmann equation with a Bhatnagar-Gross-Krook (BGK) collision operator  $\Omega_i$  (Bhatnagar *et al.* 1954) is given by

$$f_i(\mathbf{x} + \mathbf{c}_i \Delta t, t + \Delta t) - f_i(\mathbf{x}, t) = \Omega_i(\mathbf{x}, t) + F_i(\mathbf{x}, t) \Delta t, \quad (2.1)$$

with

$$\Omega_i(\mathbf{x}, t) = -\frac{\Delta t}{\tau} [f_i(\mathbf{x}, t) - f_i^{eq}(\mathbf{x}, t)], \quad (2.2)$$

and

$$f_i^{eq}(\mathbf{x}, t) = \omega_i \rho \left[ 1 + 3(\mathbf{c}_i \cdot \mathbf{u}) + \frac{9}{2}(\mathbf{c}_i \cdot \mathbf{u})^2 - \frac{3}{2}|\mathbf{u}|^2 \right], \quad (2.3)$$

where  $\tau$  is a relaxation time related to the fluid kinematic viscosity  $\nu = c_s^2 (\tau - \frac{\Delta t}{2})$ .  $c_s = \frac{1}{\sqrt{3}} \frac{\Delta x}{\Delta t}$  denotes the lattice speed of sound,  $\Delta x$  is the lattice constant,  $\omega_i$  are lattice weights,  $\mathbf{u}$  is the macroscopic fluid velocity, and  $f_i^{eq}(\mathbf{x}, t)$  is the equilibrium probability distribution function expressed in terms of a truncated expansion of the Maxwell-Boltzmann distribution valid at small Mach number ( $Ma = |\mathbf{u}|/c_s \ll 0.1$ ).  $F_i$  in the RHS of equation 2.1 accounts for an arbitrary external force and will be used here to incorporate the forces exerted by the membrane on the fluid through the immersed boundary method. For a D3Q19 LBM, the lattice weights  $\omega_i$  read as 1/3, 1/18 and 1/36 for  $i = 1$ ,  $i = 2 \dots 7$ , and  $i = 8 \dots 19$ , respectively. The macroscopic fluid density  $\rho$  and velocity  $\mathbf{u}$  are deduced from the moments of the discrete probability distribution functions as

$$\rho = \sum_{i=1}^{19} f_i(\mathbf{x}, t), \quad \text{and} \quad \mathbf{u} = \sum_{i=1}^{19} f_i(\mathbf{x}, t) \mathbf{c}_i / \rho. \quad (2.4)$$

For convenience we set the lattice constant, the time step, the fluid mass density, and the relaxation time to unity.

The fluid-membrane coupling is achieved using the immersed boundary method (IBM) introduced by Peskin (2002), where the Lagrangian massless nodes are interacting with the Eulerian fluid nodes using an interpolation function in a two-way coupling scheme: the membrane forces are distributed to the surrounding fluid nodes within the interpolation function range and then the updated fluid velocities are interpolated back to the membrane nodes using the same scheme. The distribution of the membrane forces  $\mathbf{F}_i^m$  located at position  $\mathbf{X}_i(t)$  to the adjacent fluid nodes is given by

$$\mathbf{f}(\mathbf{x}, t) = \sum_i \mathbf{F}_i^m(t) \delta(\mathbf{x} - \mathbf{X}_i(t)), \quad (2.5)$$

where  $\sum_i$  runs over the membrane nodes located within the interpolation range of a given fluid node  $\mathbf{x}$ ,  $\delta$  is a three-dimensional approximation of the Dirac delta function, and  $\mathbf{f}(\mathbf{x}, t)$  is the force density acting on the fluid at the Eulerian node  $\mathbf{x}(x_1, x_2, x_3)$ . Equation 2.5 is incorporated into equation 2.1 in a similar manner to an external body force (*e.g.* gravity) such as

$$F_i(\mathbf{x}, t) = \left( 1 - \frac{1}{2\tau} \right) \omega_i \left( \frac{\mathbf{c}_i - \mathbf{u}}{c_s^2} + \frac{\mathbf{c}_i \cdot \mathbf{u}}{c_s^4} \mathbf{c}_i \right) \cdot \mathbf{f}(\mathbf{x}, t). \quad (2.6)$$

To avoid jumps in velocities or in the applied forces occurring when the Lagrangian nodes do not coincide with the nodes of the Eulerian grid, the Dirac delta function is usually replaced with a smoother interpolation function ( $\varphi$ ) of some shape such as  $\delta(\mathbf{x}) = \varphi(x_1)\varphi(x_2)\varphi(x_3)$ . Several distribution functions have been used in the IBM literature for a wide range of applications. For detailed reviews on the IBM and its accuracy, we refer the reader to Mittal & Iaccarino (2005) among other existing works on this topic. In what follows, we use a two-point linear interpolation function as discussed in Krüger (2012),

which is given by

$$\varphi(\xi) = \begin{cases} 1 - |\xi| & \text{for } 0 \leq |\xi| \leq 1 \\ 0 & \text{for } |\xi| \geq 1 \end{cases}, \quad (2.7)$$

where  $\xi$  can denote  $x_1$ ,  $x_2$ , or  $x_3$ .

The capsule is modelled as a two-dimensional hyperelastic thin shell encapsulating an inner fluid and suspended in an outer fluid. The interior and exterior fluids are considered here to be Newtonian with the same densities and viscosities. The membrane of the capsule is discretized into a triangular mesh and endowed with a resistance to in-plane deformations. The capsule stress-free shape is initialised as a sphere in all our simulations. We should stress that the bending resistance is not considered in this study to limit the number of controlling parameters. The volume of the capsules is prescribed using a penalty function that reads as

$$E_v = \frac{\kappa_v}{2} \frac{[V - V_0]^2}{V_0}, \quad (2.8)$$

where  $\kappa_v$  is a modulus that controls the deviation from the reference volume  $V_0$  corresponding to the stress-free shape. We consider the case of a strain-hardening membrane using the hyperelastic law introduced by Skalak (1973), where the in-plane elastic deformations are governed by shear and area dilatation resistances. In terms of the deformation invariants,  $I_1 = \lambda_1^2 + \lambda_2^2 - 2$  and  $I_2 = \lambda_1^2 \lambda_2^2 - 1$ , where  $\lambda_1$  and  $\lambda_2$  are the principal stretching ratios on an element of the membrane surface, the Skalak constitutive law describing the strain energy of a membrane patch reads as

$$w_s = \frac{G_s}{4} [I_1^2 + 2I_1 - 2I_2 + CI_2^2]. \quad (2.9)$$

Here,  $G_s$  is the elastic shear modulus and  $C$  is a constant related to the strain-hardening nature of the membrane through the scaled area dilatation modulus  $G_a$  such as  $G_a/G_s = 1 + 2C$ , so to say increasing the value of  $C$  increases the local inextensibility of the membrane. In the small deformation limit,  $C$  and the surface Poisson ratio ( $\nu_s$ ) are related by  $C = \frac{\nu_s}{1-\nu_s}$  (Barthès-Biesel *et al.* (2002)).

To avoid overlap between capsules in densely packed systems, we introduce a short range repulsion force intended to mimic the normal component of the lubrication force as suggested by Glowinski *et al.* (2001) that acts when the distance between two nodes from different capsules is below the fluid resolution limit of the LBM. This force vanishes at a node-to-node distance  $d_{ij}$  above one lattice unit and is given by

$$\mathbf{F}_{rep} = \begin{cases} \bar{\epsilon} \left[ \frac{1}{d_{ij}^2} - 1 \right] \frac{\mathbf{d}_{ij}}{d_{ij}} & \text{if } d_{ij} < 1 \\ \mathbf{0} & \text{if } d_{ij} \geq 1 \end{cases}, \quad (2.10)$$

where  $\bar{\epsilon}$  is the interaction strength. At the beginning of the simulations, the capsules are initialised with a scaled radius and seeded to random positions within the physical domain. The radius of the capsule is increased in time with a fixed growth rate until reaching the desired size which results in a densely packed suspension of particles with volume fractions up to  $\phi = 0.5$  in this study. During this process, the capsules are subject to the deformations resulting from the particle-particle interaction as described earlier. The Reynolds number at the scale of the particle is defined by

$$Re_p = \frac{\rho \dot{\gamma} r^2}{\mu_0}, \quad (2.11)$$

where  $\rho$  and  $\mu_0 = \rho\nu$  are the fluid density and dynamic viscosity, and  $\dot{\gamma}$  is the shear rate.

In all our simulations, the particle Reynolds number is kept below 0.03. The capillary number describing the deformation of a capsule in a shear flow is written as

$$Ca = \dot{\gamma}\tau_{el}, \quad (2.12)$$

where  $\tau_{el} = \mu_0 r / G_s$  is a time scale associated to the elasticity of the capsule. To determine the bulk rheological properties, we start by evaluating the average particle stress tensor by following the work of Batchelor (1970). The average particle stress is given by

$$\Sigma_{ij}^p = \frac{1}{N} \sum_{\alpha=1}^N n S_{ij}^\alpha = -\frac{1}{V_D} \sum_{\alpha=1}^N \int_A \frac{1}{2} \{F_i^{m,\alpha} X_j^\alpha + F_j^{m,\alpha} X_i^\alpha\} dA, \quad (2.13)$$

where  $i$  and  $j$  are indices referring to Cartesian directions,  $\sum_{\alpha=1}^N$  is a sum over the number of particles  $N$  in the averaging volume  $V_D$ ,  $n$  the number density,  $\mathbf{S}$  the particle stresslet,  $\mathbf{X}$  is a Lagrangian node on the membrane and  $\mathbf{F}^m$  the surface force density exerted by the membrane on the fluid. The relative viscosity of the suspension  $\mu_r$  is expressed as

$$\mu_r = \frac{\Sigma_{13}^p}{\mu_0 \dot{\gamma}}. \quad (2.14)$$

The normal stress differences and the particle pressure can be deduced from the average particle stress tensor such as

$$N_1 = \Sigma_{11}^p - \Sigma_{33}^p, \quad N_2 = \Sigma_{33}^p - \Sigma_{22}^p, \quad \text{and} \quad \Pi = -\frac{1}{3} \text{Tr}(\Sigma^p). \quad (2.15)$$

The deformation of a capsule in the shear plane can be described using a dimensionless number introduced for droplets by Taylor (1934). The Taylor deformation parameter is defined as

$$D = \frac{r_1 - r_3}{r_1 + r_3}, \quad (2.16)$$

where  $r_1$  and  $r_3$  are the major and minor semi-axes of an ellipsoid having the same tensor of inertia as the deformed capsule. This method has been described in Ramanujan & Pozrikidis (1998) and used extensively in the literature of capsules (Lac *et al.* (2004); Li & Sarkar (2008); Le (2010); Krüger *et al.* (2014); Wouters *et al.* (2019)). The ellipsoid radii are defined as

$$r_1 = \sqrt{\frac{5}{2\rho V} (I_2 + I_3 - I_1)}, \quad r_2 = \sqrt{\frac{5}{2\rho V} (I_1 + I_3 - I_2)}, \quad r_3 = \sqrt{\frac{5}{2\rho V} (I_1 + I_2 - I_3)}, \quad (2.17)$$

where  $I_1$ ,  $I_2$ , and  $I_3$  are the eigenvalues of the tensor of inertia.

The rheology and microstructure of suspensions of strain-hardening capsules up to a volume fraction of 0.5 are studied for capillary numbers ranging from  $Ca = 0.1$  to 1. The computational domain is a cube with a side length  $L = 128\Delta x$ . The domain is biperiodic along the flow and vorticity directions, respectively  $x$  and  $y$  directions, and bounded by two planar walls in the  $z$  direction. We impose a velocity boundary condition at the walls to generate the driving shear flow as described in Hecht & Harting (2010). The number of particles is varied from 1 to 500 corresponding to  $\phi \approx 0.001$  and  $\phi \approx 0.5$ , respectively. Each particle is discretized with 1280 triangles and 642 nodes, and initialized as a sphere with a radius  $R = 8\Delta x$ . The position of the particles is updated using a forward Euler integration scheme. To limit the number of parameters influencing the capsule deformation and rheology, the bending stiffness is not taken into account and the viscosity contrast between the inner and outer fluids is fixed to unity. The relative error on the capsule's volume defined as  $\epsilon_V = |V - V_0|/V_0$  is below 0.03% in all simulations.

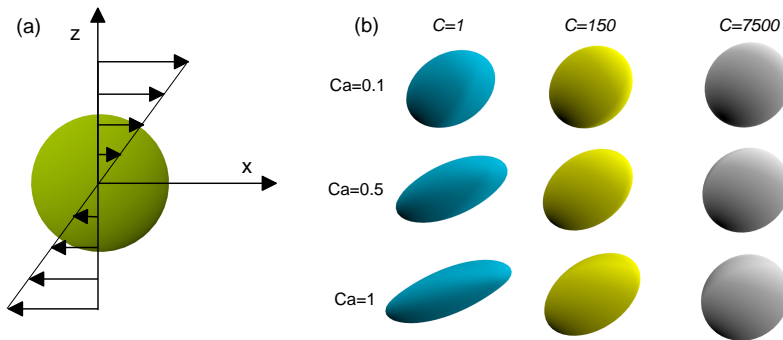


FIGURE 1. Schematic of a single capsule in a shear flow showing the initial (a) and steady-state configurations (b) for different values of  $C$  and  $Ca$ .

For suspensions, the measured quantities are obtained from an average over the number of particles and over time. The time average is performed after the initial transient state corresponding to approximately the first 10 strain units. A test simulation of a domain size of  $256^3$  lattice sites with 1200 capsules corresponding to  $\phi \approx 0.15$  and for  $Ca = 0.5$  showed that the relative error with respect to a  $128^3$  system is around 0.7% for the mean Taylor deformation index and 0.6% for the relative viscosity. Each simulation required 64 cores on a current supercomputer and ran for a few million time steps corresponding to one to two weeks of calculation time depending on the number of particles and the capillary number. Details on the performance of our code can be found in Aouane *et al.* (2018).

### 3. Results

#### 3.1. Behaviour of a single capsule in a shear flow

In order to validate our approach, we first limit our simulations to the case of single initially spherical Skalak capsules. Our simulation domain is bounded by two parallel walls and the confinement is set to  $C_n = 2R/L = 0.125$ , so that the effect of the boundaries can be neglected. A schematic representation of the simulation setup, together with examples of steady state shapes for different  $Ca$  and  $C$ , are depicted in Fig. 1. The intrinsic viscosity, the normal stress difference, the steady Taylor deformation index and the orientation angle between the major axis of the particle and the flow direction as functions of  $Ca$  (for different values of  $C$ ) are plotted in Fig. 2 and compared with numerical results obtained using the boundary element method (Lac *et al.* (2004)) and the front-tracking method (Bagchi & Kalluri (2010)), showing good agreement. We next move to explore systematically the parameter space spanned by  $(Ca, C)$ , with  $Ca \in [0.1; 1]$  and  $C \in [1; 7500]$ . The corresponding data on steady-state elongation, inclination angle, intrinsic viscosity and first normal stress difference are reported in Fig. 3. We see, from the symbols in Fig. 3(c), at fixed  $C$ , that  $[\mu]$  decreases with  $Ca$ , denoting a shear-thinning character. The latter, in turn, appears to be directly correlated to an increase of the elongation of the capsule (Fig. 3(a)) and a decrease of its orientation with respect to the flow direction (Fig. 3(b)), similarly to what has been reported for drops, vesicles, and strain-softening capsules. Moreover, a clear effect of  $C$  on the various observables can be detected: as  $C$  grows, their dependence on  $Ca$  gets weaker. In particular, the steady Taylor parameter  $D$  suggests that the particle is less and less deformed, i.e. it approaches the limit of a rigid sphere. Correspondingly,  $[\mu]$  varies less and less with  $Ca$  and eventually the shear-thinning is suppressed. For sufficiently large  $C$ , then, a very dilute suspension

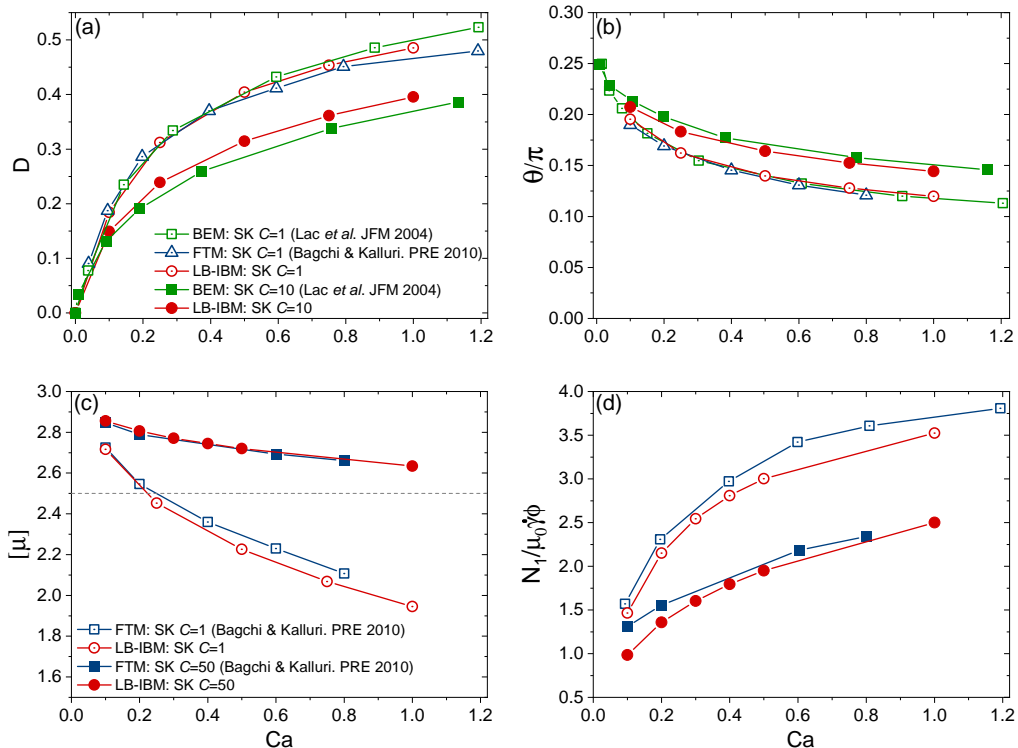


FIGURE 2. Steady Taylor deformation (a), inclination angle (b), intrinsic viscosity (c), and first normal stress difference (d) of a single capsule under a shear flow. The open and full symbols in (a) and (b) are for  $C = 1$  and  $C = 10$ , respectively, and for  $C = 1$  and  $C = 50$  in (c) and (d). BEM denotes the boundary element simulations of Lac *et al.* (2004), and FTM the front-tracking method of Bagchi & Kalluri (2010). LB-IBM are the numerical results obtained using our lattice Boltzmann code. The dashed line in (c) indicates the value of the intrinsic viscosity of a dilute suspension of rigid spheres. The legends for (b) and (d) are indicated in (a) and (c), respectively.

of strain-hardening capsules tends to behave rheologically as a suspension of rigid spheres (notice also that  $N_1$  tends to zero, Fig. 3(d)), albeit with an intrinsic viscosity surprisingly slightly larger than the Einstein coefficient  $[\mu] = 5/2$  (we found, as a limiting value for  $C \gg 1$ ,  $[\mu] \approx 2.8$ ; see also Bagchi & Kalluri (2010) for comparison).

### 3.2. Suspensions: structure

We investigate the multi-particle case and the dependence of particle shape and suspension rheological properties on the parameters describing the system, namely  $Ca$ ,  $C$ , and  $\phi$ . We scan the parameter space  $(Ca, C, \phi)$  within the ranges  $Ca \in [0.1, 1]$ ,  $C \in [10^{-3}, 7.5 \times 10^3]$  and  $\phi \in [10^{-3}, 0.5]$ . Examples of steady-state configurations of the suspension are shown in Fig. 4, for fixed  $Ca = 1$ ,  $\phi = 0.5$  and for four different values of  $C = 0.1, 10, 150, 7500$ .

In this subsection we focus on particle morphologies, characterized in terms of the Taylor deformation parameter and the semi-axes of the equivalent ellipsoid, whereas in the next one we will study the rheological properties of the suspensions, highlighting their relations with the structure. Analogously to the single particle case, the mean Taylor parameter  $\langle D \rangle$  of the suspension decreases with increasing  $C$  (Fig. 5(a)), with a steepest descent for  $1 < C < 10^3$ , which confirms that capsules become less deformable and tend



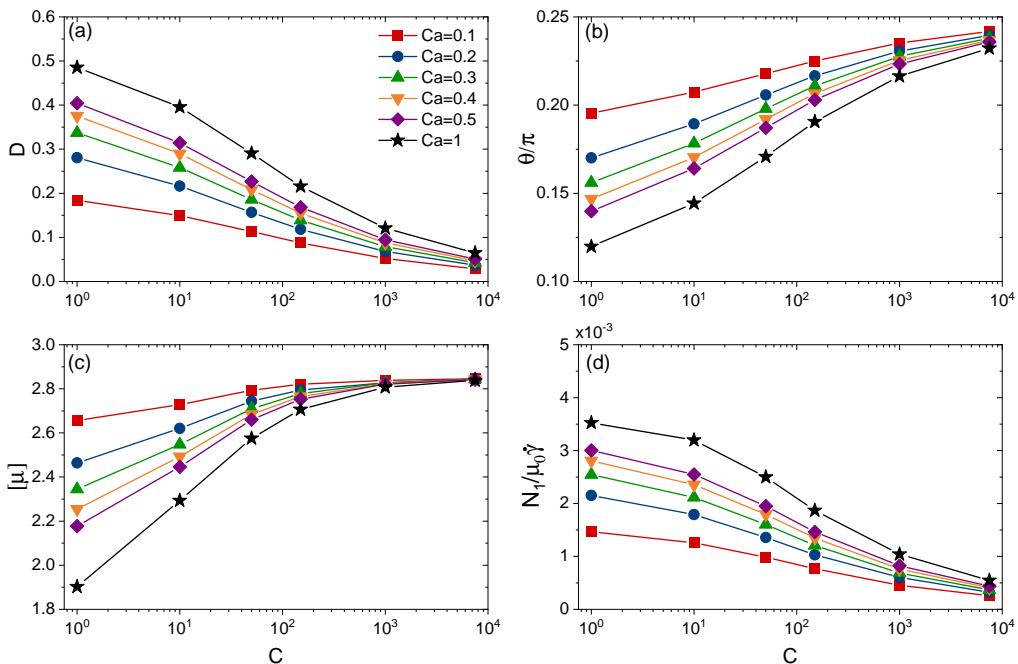


FIGURE 3. Effect of the membrane area incompressibility on the steady-state shape (a), orientation (b), intrinsic viscosity (c), and first normal stress difference (d) of a single Skalak capsule under a shear flow for different capillary numbers. The legend is given in (a).

to resemble rigid particles. We recall, though, that such a parameter contains information only on two of the three semi-axes of the equivalent ellipsoid. To get a deeper insight, then, we present all three of them separately in Fig. 5(b-d). Interestingly, a non-monotonic behaviour is found for  $\langle r_1 \rangle$  and  $\langle r_2 \rangle$  (the semi-axes in the flow and vorticity directions, respectively) for  $0.1 < C < 10$ . In particular, for decreasing  $C < 10$ ,  $\langle r_2 \rangle$ , whose direction is orthogonal to the elongational one, grows. Moreover,  $\langle r_2 \rangle$  stays always larger than  $\langle r_3 \rangle$ , indicating that particles, on average, are not spheroids (eventually, for very large  $C$  particles approach the undeformable limit and the quasi-spherical shape,  $\langle r_i \rangle \rightarrow r$  for  $i = 1, 2, 3$ , is recovered). In this sense, capsules display a lower level of symmetry than droplets, which is to be attributed to the non-linear elastic characteristics of the membrane. Notice, in fact, that the behaviour persists across the various volume fractions explored, even for the lowest  $\phi$  (corresponding to the single particle case), suggesting that the effect originates from the properties of the single particle stress tensor.

Next, we consider how the particle deformation depends on the applied load, for given material properties.

It is tempting, first of all, to investigate how the peculiar behaviour for small/moderate  $C$ 's shows up across different shear values. In figure 6(a-c) we report the variation of  $r_i$  for single capsules with  $C = 0.1, 1, 10$ , as a function of  $Ca$ . As  $Ca$  increases, the capsules get, obviously, more elongated in the extensional flow direction ( $r_1$  grows), but the two minor semi-axes display opposite trends, depending on the value of  $C$ : while  $r_3$ , as expected, decreases (for all  $C$ ),  $r_2$  (the one aligned with the vorticity direction) grows for  $C < 1$ . For the smallest  $C$  considered,  $C = 0.1$ , we need, therefore, to find an equivalent breadth,  $r_{\perp}^{(eq)}$  quantifying the degree of shrinkage or expansion of the capsule in the equatorial plane. We define this  $r_{\perp}^{(eq)}$  as the ratio of the length of the membrane cross-section (an ellipse) over  $2\pi$  (such that it would be precisely the minor axis, if the capsule were a prolate spheroid),

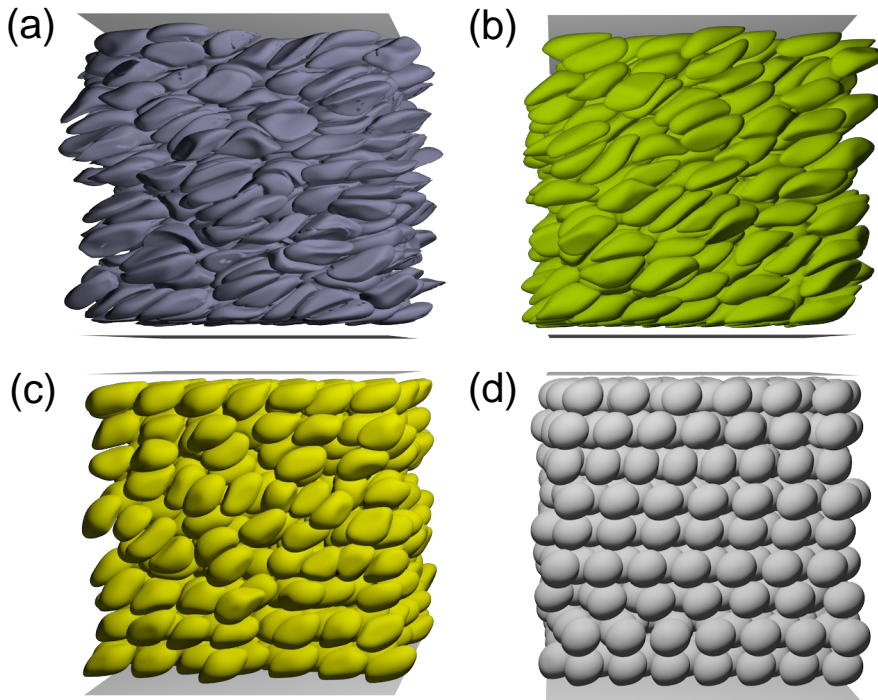


FIGURE 4. Steady-state configurations for  $\phi = 0.5$ ,  $Ca = 1$  and  $C = 0.1$  (a),  $C = 10$  (b),  $C = 1.5 \times 10^2$  (c) and  $C = 7.5 \times 10^3$  (d).

i.e.  $r_{\perp}^{(\text{eq})} = \frac{4r_2\mathcal{E}(\epsilon(r_2, r_3))}{2\pi}$ , where  $\mathcal{E}(x)$  is the complete elliptic integral of the second kind (Abramowitz & Stegun (2012)) and  $\epsilon(r_2, r_3) = \sqrt{1 - \left(\frac{r_3}{r_2}\right)^2}$  is the eccentricity of the ellipse. In figure 6(d), we plot the transversal deformation, represented by  $r_{\perp}^{(\text{eq})}$  versus the elongation,  $r_{\parallel} \equiv r_1$ , both normalised by the rest radius  $r$ , for the capsule with  $C = 0.1$ . It can be seen that, although  $r_{\perp}^{(\text{eq})}/r$  never exceeds 1, i.e. overall the membrane cross-section shrinks with respect to the equilibrium shape, there is a range of  $Ca$  for which it expands as the capsule is elongated. This is an intriguing behaviour, in fact the opposite of the slope of the curve in Fig. 6(d),  $\tilde{\nu}_s = -\frac{dr_{\perp}^{(\text{eq})}}{dr_{\parallel}}$ , can be interpreted as a *local* Poisson's ratio, which is negative for  $1.3r \lesssim r_{\parallel} \lesssim 1.7r$ . This observation hints at a sort of local (in shear) “auxeticity” (Evans *et al.* (1991)) of membranes obeying a Skalak-type constitutive law with low values of the membrane inextensibility parameter.

In figure 7(a) we show the average Taylor deformation parameter as function of  $Ca$ , for various  $\phi$ 's. Two sets of data corresponding to  $C = 50$  (closed symbols) and  $C = 150$  (open symbols) are reported. The deformation grows as  $\langle D \rangle \sim Ca$  for small capillary numbers, as expected, and then sub-linearly as the  $Ca$  increases (eventually we observe a logarithmic dependence  $\langle D \rangle \sim \log(Ca)$ , in agreement with previous numerical (Dodson III & Dimitrakopoulos 2010) and experimental (Hardeman *et al.* 1994) findings), reflecting the strain-hardening character of the capsules. It can be asked whether one may find a functional form that allows to recast the variability among curves into a single curve

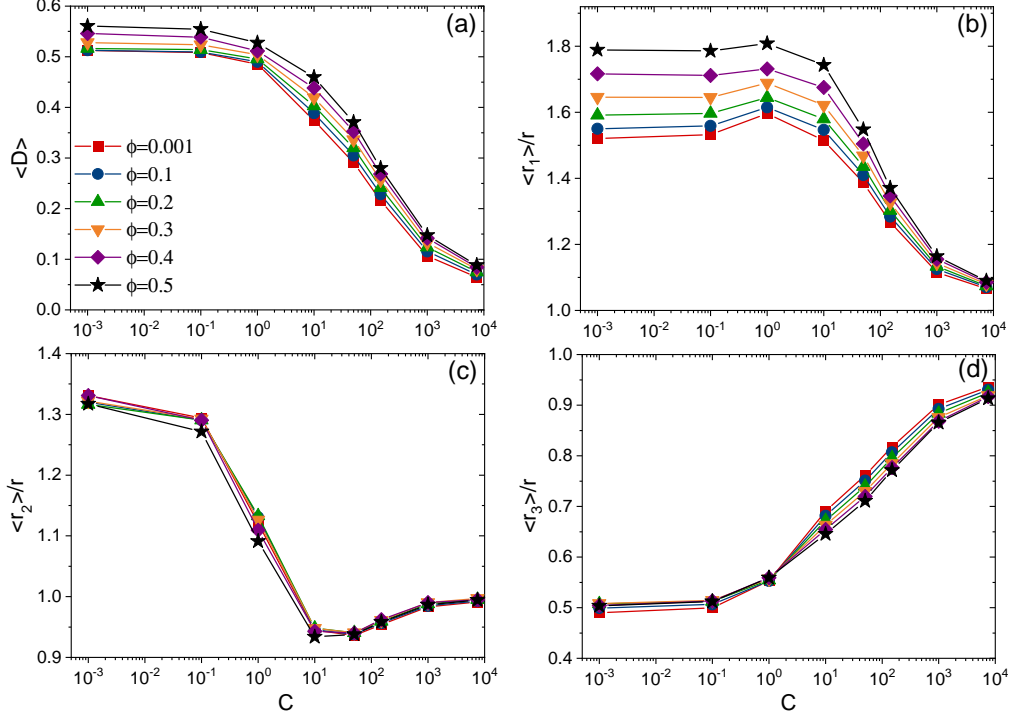


FIGURE 5. Steady-state Taylor deformation parameter (a). Steady-state mean semi-axes of the capsules normalized by the reference radius as function of  $C$  for different values of  $\phi$  (b-d). The legend is indicated in (a).

shape parameter,  $Ca^*(\phi, C)$ , that is

$$\langle D \rangle \equiv \mathcal{D}(Ca, \phi, C) = Ag \left( \frac{Ca}{Ca^*(\phi, C)} \right), \quad (3.1)$$

where  $A$  is a constant prefactor and the function  $g(x)$  has to be chosen such that it reproduces and connects both behaviours at small and large  $Ca$ , that is  $g(x) \sim x$  as  $x \rightarrow 0$  and  $g(x) \sim \log(x)$  for  $x \gg 1$ . This is indeed possible and we show it in figure 6(a). There, the fits, indicated by the dashed lines, are obtained from equation (3.1), choosing for the function  $g$  the expression  $g(x) = \log(1 + x)$ , with the same  $A = 0.1$  and, from bottom to top,  $Ca^* = 0.13$ ,  $Ca^* = 0.07$ , and  $Ca^* = 0.037$ , respectively. For a fixed capillary number,  $\langle D \rangle$  increases linearly with the volume fraction  $\phi$ , similarly to suspensions of drops and neo-Hookean capsules (Loewenberg & Hinch 1996; Frijters *et al.* 2012; Matsunaga *et al.* 2016). Conversely, the larger is the membrane inextensibility  $C$ , the less deformed are the capsules.

Given the self-similar form of (3.1), we would like to find a universal curve for  $\langle D \rangle$ , through a proper definition of an effective capillary number  $Ca_{\text{eff}}$ . The enhancement of deformation with  $\phi$  can be interpreted as an effect of larger viscous stresses around the particle, due to the fact that the effective viscosity of the suspension increases with the volume fraction (this aspect will be discussed in more detail in the next subsection). This suggests that we should replace, in  $Ca_{\text{eff}}$ , the “bare” dynamic viscosity with the effective one,  $\mu_0 \rightarrow \mu_{\text{eff}} = \mu_0(1 + [\mu]\phi)$ . Here we assume, for simplicity, linearity in  $\phi$  and a constant (with  $Ca$  and  $C$ ) intrinsic viscosity, equal to its large  $C$  limit,  $[\mu] \approx 2.8$  (see section 3.1).

Furthermore, we note that for a non-zero membrane inextensibility, it is more ap-

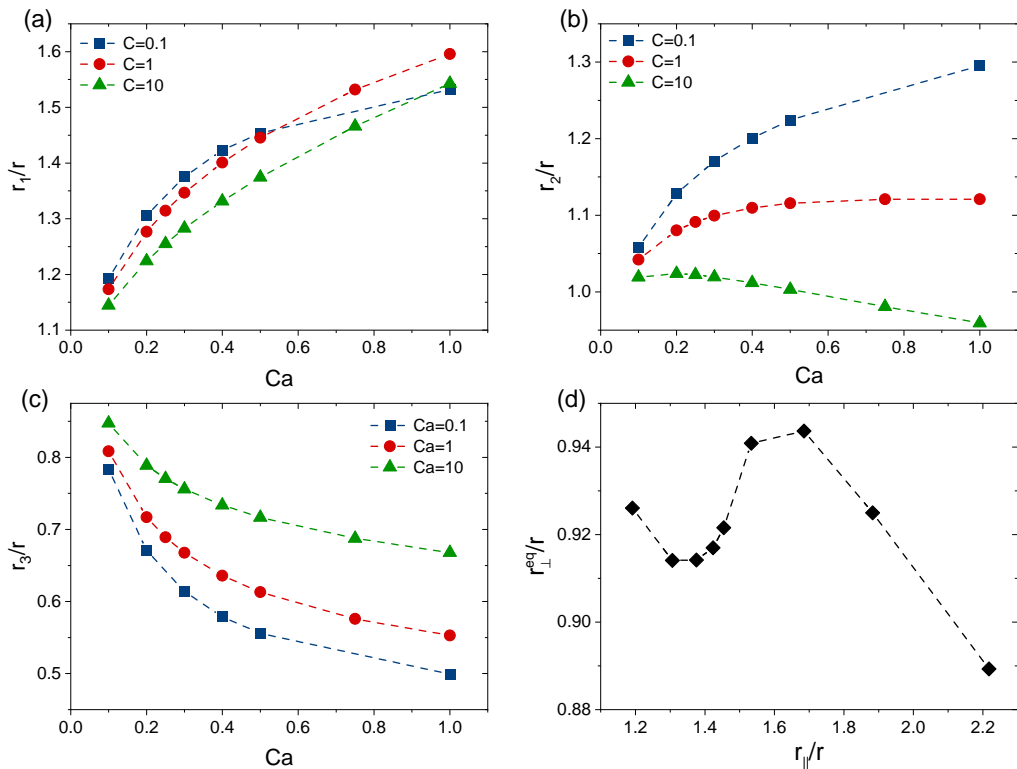


FIGURE 6. Steady-state semi-axes (normalized by the reference radius) as a function of  $Ca$  for capsules with  $C = 0.1, 1, 10$  (a-c) (the legend is indicated in (a)). Transversal deformation versus elongation (normalized by the reference radius) for a capsule with  $C = 0.1$  (c).

proprate to base the capillary number on the Young's modulus instead of the shear modulus (Barthès-Biesel & Rallison (1981)). We propose to replace  $G_s$  with  $E_s = \frac{(2+4C)}{(1+C)} G_s$ . However, this might not be sufficient. In fact, the imposed constraint of volume conservation, for a spherical equilibrium shape, effectively entails an extra-tension on the surface, since the capsules tend to become essentially undeformable as the area dilatation modulus is increased. This can be accounted for by the substitution

$$E_s \rightarrow E_s^{(\text{eff})} = \frac{(2+4C)}{(1+C)} G_s^{(\text{eff})} = \frac{(2+4C)}{(1+C)} (1 + \beta C) G_s \quad (3.2)$$

( $\beta$  being a free parameter, which we set hereafter to  $\alpha = 0.07$ ) in the effective capillary number, which then finally reads

$$Ca_{\text{eff}}(\phi, C) = \frac{\mu_{\text{eff}} \dot{\gamma} r}{E_s^{(\text{eff})}} = \frac{(1 + [\mu]\phi)(1+C)}{(2+4C)(1+\beta C)} \left( \frac{\mu_0 \dot{\gamma} r}{G_s} \right) \equiv \frac{(1 + [\mu]\phi)(1+C)}{(2+4C)(1+\beta C)} Ca. \quad (3.3)$$

When plotted as function of  $Ca_{\text{eff}}$ , the values of  $\langle D \rangle$  for different  $\phi$  and  $C$  collapse onto a single master curve, as shown in figure 7(b). Such curve can be also fitted using (3.1), with  $A = 0.1$  and  $Ca_{\text{eff}}^* = 4 \times 10^{-3}$ . Notice that the existence of a single  $Ca_{\text{eff}}^*$  capable to fit all data sets upon the rescaling (3.3) is equivalent to say that the dependence of the curve-shape parameter  $Ca^*$  on  $Ca$  and  $C$  is such that  $Ca^* \propto \frac{G_s^{(\text{eff})}(C)}{\mu_{\text{eff}}(\phi)}$ .

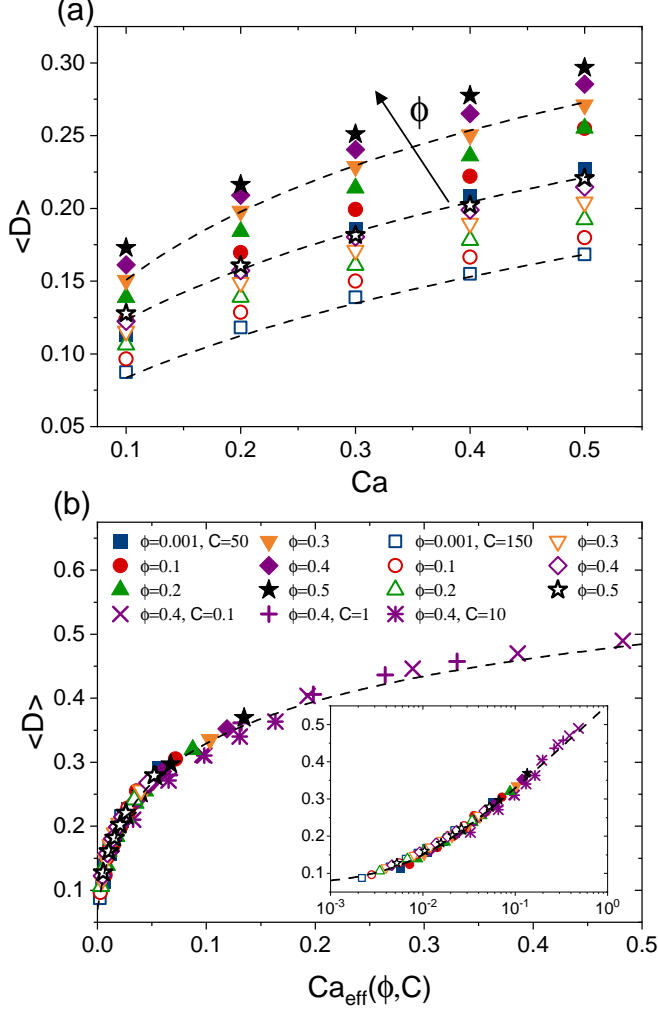


FIGURE 7. (a) Mean Taylor deformation parameter for a suspension of strain-hardening capsules as a function of  $Ca$ , for two values of membrane extensibility,  $C = 50$  (filled symbols) and  $C = 150$  (open symbols). The dashed lines are fits of the numerical data using equation (3.1) with  $A = 0.1$  and (from bottom to top)  $Ca^* = 0.13$ ,  $Ca^* = 0.07$  and  $Ca^* = 0.037$ , respectively. The arrow indicates a growing volume fraction  $\phi$ . (b) Mean Taylor deformation parameter as a function of the effective capillary number, Eq. (3.3). The dashed line corresponds to the fitting function (3.1) ( $A_{\text{eff}} = 0.1$  and  $Ca_{\text{eff}}^* = 4 \times 10^{-3}$ ). Inset: Lin-Log plot of  $\langle D \rangle$  vs  $Ca_{\text{eff}}$ , highlighting the logarithmic behaviour for  $Ca_{\text{eff}} > Ca_{\text{eff}}^*$ . The legend is indicated in (b).

### 3.3. Suspensions: rheology

We now consider the rheological response of the system, assessed by the suspension relative viscosity and normal stress differences. In figure 8, we plot  $N_1$  and  $N_2$  at  $Ca = 1$  as a function of the membrane inextensibility for various volume fractions. We see that both (though,  $N_2$  only weakly) show a non-monotonic dependence on  $C$ , a behaviour that is enhanced as  $\phi$  is increased. In particular,  $N_1$  initially grows with  $C$ , reaches a peak at  $C \approx 10$ , and then starts to decrease. We argue that these features might be correlated to the peculiar anisotropisation of capsules, as depicted by the analysis in figure 5. For

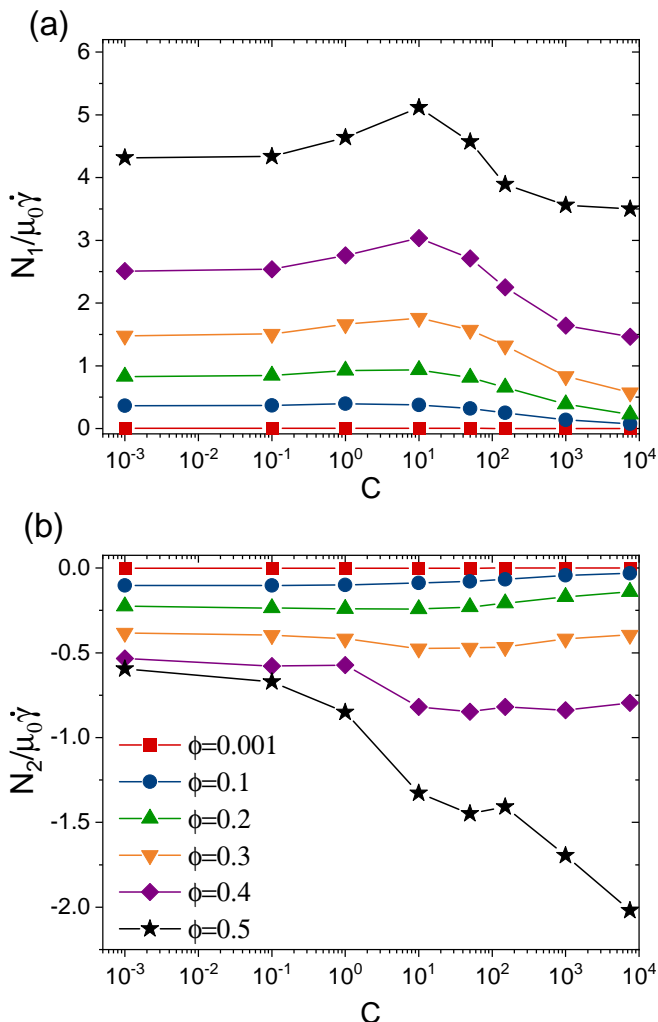


FIGURE 8. First (a) and second (b) normal stress differences as function of  $C$ . The legend is shown in (b).

emulsions and strain-softening capsules, the magnitude of  $N_1$  is significantly larger than the magnitude of  $N_2$ , whereas the opposite is true for suspensions of rigid particles.  $N_1$  and  $N_2$  are known to be correlated to hydrodynamic interaction, and particle-particle collisions, respectively (Guazzelli & Pouliquen (2018)). We find that for strain-hardening capsules  $N_1$  is positive while  $N_2$  has a negative sign, and the magnitude of  $N_1$  is larger than  $N_2$ . Interestingly, the ratio of magnitudes  $|N_1|/|N_2|$  diminishes with the increase of  $C$ . Therefore, it is in principle possible, by tuning their deformability through  $C$ , to cause collections of such soft particles to behave rheologically more as emulsion-like or suspension-like systems.

The relative viscosity  $\mu_r$  of suspensions of capsules with  $C = 0.1, 1, 10, 150$  is reported in figure 9(a) as a function of the volume fraction  $\phi$ , with  $Ca$  ranging in  $[0.1, 0.5]$ . As for other types of suspensions of rigid or deformable particles, the growth of  $\mu_r$  is approximately linear for  $\phi \lesssim 0.1$  and then becomes steeper. The shear-thinning character of the suspension of capsules can be appreciated: for a given volume fraction, in fact,  $\mu_r$

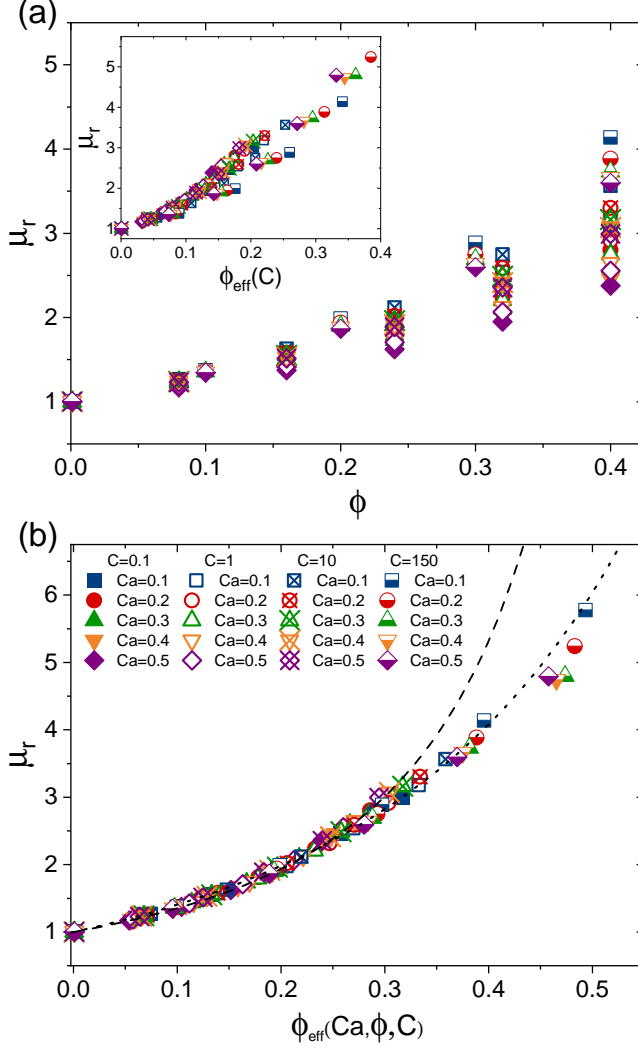


FIGURE 9. (a) Relative viscosity as a function of the volume fraction for different  $Ca$  and  $C$ . The inset shows  $\mu_r$  plotted as function of the effective volume fraction as defined in equation (3.6). The legend of (a) is shown in (b). (b) Relative viscosity as a function of the effective volume fraction (see equation (3.7)). The dashed line corresponds to a fit of the numerical data using equation (3.8), with  $B = 1.4$ , and  $\Phi_m = 0.7$ . Same for the dotted line but with  $B = 1.7$ , and  $\Phi_m = 1.2$ .

tends to decrease with  $Ca$  (the larger  $\phi$  the more evident is the shear-thinning), but the spread is reduced for larger  $C$ . In order to find a universal behaviour of the relative viscosity across the various shear rates, recently Rosti *et al.* (2018) introduced the notion of a reduced *effective* volume fraction, calculated using for the capsule volume (when they are in the deformed state), that of a sphere with a radius equal to the smallest particle semi-axis  $r_3$ , i.e.  $\Phi_{\text{eff}} = \frac{4}{3}\pi r_3^3$ . The rationale behind this approach is that the dynamically “active” direction is the velocity gradient (wall-normal direction) and, since the deformed particles do not tumble and tend to align with the flow direction, then the relevant length is the minor axis. For  $r_3$ , the average value as measured in the

simulations was taken. Here, we propose to relate  $r_3$  to the radius at rest  $r$  through the Taylor deformation parameter  $D$ . To this aim, let us assume the particles to be prolate ellipsoids with  $r_1 > r_2 = r_3$  (this is an approximation that allows to close the problem, although we know that the specific relation among the three axes depends on the value of membrane inextensibility  $C$ ).  $r_1$  and  $r_3$  enter in the expression of  $D$  (equation (2.16)), that can be inverted as

$$r_1 = \frac{1+D}{1-D} r_3. \quad (3.4)$$

Due to volume conservation we have  $r^3 = r_1 r_3^2$  and therefore  $r^3 = \frac{1+D}{1-D} r_3^3$ , which implies

$$r_3 = \left( \frac{1-D}{1+D} \right)^{1/3} r. \quad (3.5)$$

If we now define, as in Rosti *et al.* (2018), the effective volume fraction as  $\Phi_{\text{eff}} \equiv \frac{4}{3} \pi \langle r_3 \rangle^3 n$  and assume (3.5) to be valid also for average quantities in the suspension, we get

$$\Phi_{\text{eff}} = \frac{1 - \langle D \rangle}{1 + \langle D \rangle} \phi. \quad (3.6)$$

As we learned from the previous section,  $\langle D \rangle$ , in turn, depends on  $\phi$ , on the capillary number and on  $C$ . If we plug equation (3.1) inside (3.6), with the rescaled effective capillary number, (3.3), and we plot  $\mu_r$  as a function of the obtained  $\Phi_{\text{eff}}$ , we do not observe, though, a very good overlap of the data (see inset of Fig. 9(a)). We ascribe this partial failure to the fact that our strain-hardening capsules are not precisely aligned with the flow direction, especially for the largest values of  $C$  (see Fig. 2(b)). Consequently, the relevant, flow-orthogonal, length is not exactly  $r_3$ , but the vertical semi-axis of the ellipse, resulting as the section of the particle ellipsoid on a plane perpendicular to the flow direction (and crossing its centre). It is easy to show, by geometrical arguments, that such length is  $\ell = r_3 \sqrt{\frac{1+b^2}{1+\left(\frac{r_3}{r_1}\right)^2 b^2}}$ , where  $b = \tan(\theta)$ , and  $\theta$  is the inclination angle.

If we define the effective volume fraction in terms of this length (and recalling that  $r_3/r_1 = (1-D)/(1+D)$ ), equation (3.6) becomes

$$\Phi_{\text{eff}} = \frac{1 - \langle D \rangle}{1 + \langle D \rangle} \left( \frac{1 + b^2}{1 + \left( \frac{1 - \langle D \rangle}{1 + \langle D \rangle} \right)^2 b^2} \right)^{3/2} \phi. \quad (3.7)$$

The parameter  $b$  itself depends, through  $\theta$ , on  $Ca$  and  $C$ . However, for simplicity, we consider it here as a fit constant, taking for  $\theta$  values restricted to the range in Fig. 2(b). In particular, for  $\theta = \frac{\pi}{5}$  ( $b \approx 0.726$ ), we get a nice collapse of all data sets onto a single master curve which can be well fitted, among others, with an Eilers function (Eilers (1941))

$$\mu_r(\Phi_{\text{eff}}) = \left[ 1 + \frac{B \Phi_{\text{eff}}}{1 - \frac{\Phi_{\text{eff}}}{\Phi_m}} \right]^2, \quad (3.8)$$

with parameters  $B = 1.4$  and  $\Phi_m = 0.7$  (figure 9(b)). Choosing  $B = 1.7$  and  $\Phi_m = 1.2$  also the branch at large  $\Phi_{\text{eff}}$  can be fitted, but these are somehow not sound values. We argue, instead, that the deviations from the Eilers fit (which occur for the set of data corresponding to the largest  $C = 150$  and  $\phi = 0.4, 0.5$ ) are due to the fact that under these conditions important hydrodynamic correlations emerge which cannot be simply adhered to a reduced volume effect. Let us stress that the relation (3.6), as much as



in the approach of Rosti *et al.* (2018), needs an empirical input (the function  $g(x)$  in (3.1)). However, for small effective capillary number, it is possible to approximate  $g$  with its linear part, thus providing a closed and explicit expression for  $\Phi_{\text{eff}}(Ca, C, \phi)$  and, consequently, an explicit dependence of the relative viscosity  $\mu_r$  on  $Ca$ ,  $C$  and  $\phi$ .

## 4. Conclusions

The rheology of a suspension of strain-hardening capsules is investigated numerically from the dilute to the concentrated regimes in a simple shear flow. We have addressed the role of the capillary number, the membrane inextensibility and the volume fraction on the microstructure and the global rheology. Our results for a single strain-hardening capsule show that the particle deformation diminishes drastically with the increase of membrane inextensibility, and as a consequence the shear-thinning behaviour is hindered. This transition is enhanced with the increase of the volume fraction. As a consequence, a non-monotonic behaviour of the normal stresses is observed, while the viscosity shows a non-linear monotonic dependence on the membrane inextensibility. Last but not least, the viscosity of a suspension of strain-hardening capsules with an average ellipsoidal steady-state shape shows a universal behaviour across the various shear rates and membrane inextensibility range explored in this study when including the changes in the orientation and elongation of the particles in the definition of the effective volume fraction. The viscosity can then still be approximated by an Eilers or other equivalent equation even in the concentrated limit.

## Acknowledgments

The authors acknowledge financial support by the Deutsche Forschungsgemeinschaft (DFG) within the Cluster of Excellence “Engineering of Advanced Materials” (project EXC 315) (Bridge Funding), and within the research unit FOR2688 “Instabilities, Bifurcations and Migration in Pulsatile Flows” by the grant (HA4382/8-1). This work was also supported by the Competence Network for Scientific High-Performance Computing in Bavaria (KONWIHR III, project “Dynamics of Complex Fluids”), and the European Cooperation in Science and Technology (COST) Action MP1305: “Flowing Matter”. The authors gratefully acknowledge the computing time granted by the John von Neumann Institute for Computing (NIC) and provided on the supercomputer JURECA at Jülich Supercomputing Centre (JSC), and by the High Performance Computing Center Stuttgart (HLRS) on the Hazel Hen supercomputer.

Declaration of Interests. The authors report no conflict of interest.

## REFERENCES

- ABRAMOWITZ, M. & STEGUN, I. A. 2012 *Handbook of Mathematical Functions*. Springer Science & Business Media.
- AOUANE, O., XIE, Q., SCAGLIARINI, A. & HARTING, J. 2018 Mesoscale simulations of Janus particles and deformable capsules in flow. In *High Performance Computing in Science and Engineering'17*, pp. 369–385. Springer.
- BAGCHI, P. & KALLURI, R. M. 2010 Rheology of a dilute suspension of liquid-filled elastic capsules. *Phys. Rev. E* **81** (5), 056320.
- BARTHÉS-BIESEL, D. 2016 Motion and deformation of elastic capsules and vesicles in flow. *Ann. Rev. Fluid Mech.* **48**, 25–52.

- BARTHÈS-BIESEL, D., DIAZ, A. & DHENIN, E. 2002 Effect of constitutive laws for two-dimensional membranes on flow-induced capsule deformation. *J. Fluid Mech.* **460**, 211–222.
- BARTHÈS-BIESEL, D. & RALLISON, J. M. 1981 The time-dependent deformation of a capsule freely suspended in a linear shear flow. *J. Fluid Mech.* **113**, 251–267.
- BATCHELOR, G. K. 1970 The stress system in a suspension of force-free particles. *J. Fluid Mech.* **41** (3), 545–570.
- BATCHELOR, G. K. & GREEN, J. T. 1972 The determination of the bulk stress in a suspension of spherical particles to order  $c^2$ . *J. Fluid Mech.* **56** (3), 401–427.
- BENZI, R., SUCCI, S. & VERGASSOLA, M. 1992 The lattice Boltzmann equation: theory and applications. *Phys. Rep.* **222** (3), 145–197.
- BHATNAGAR, P. L., GROSS, E. P. & KROOK, M. 1954 A model for collision processes in gases. i. small amplitude processes in charged and neutral one-component systems. *Physical Review* **94** (3), 511.
- CLAUSEN, J. R., REASOR, D. A & AIDUN, C. K. 2011 The rheology and microstructure of concentrated non-colloidal suspensions of deformable capsules. *J. Fluid Mech.* **685**, 202–234.
- DE COCK, L. J., DE KOKER, S., DE GEEST, B. G., GROOTEN, J., VERVAET, C., REMON, J. P., SUKHORUKOV, G. B. & ANTIPINA, M. N. 2010 Polymeric multilayer capsules in drug delivery. *Angew. Chem. Int. Ed.* **49** (39), 6954–6973.
- DODSON III, W. R. & DIMITRAKOPOULOS, P. 2008 Spindles, cusps, and bifurcation for capsules in stokes flow. *Phys. Rev. Lett.* **101** (20), 208102.
- DODSON III, W. R. & DIMITRAKOPOULOS, P. 2010 Tank-treading of erythrocytes in strong shear flows via a nonstiff cytoskeleton-based continuum computational modeling. *Biophys. J.* **99** (9), 2906 – 2916.
- DONBROW, M. 1991 *Microcapsules and nanoparticles in medicine and pharmacy*. CRC press.
- EILERS, VON H. 1941 Die Viskosität von Emulsionen Hochviskoser Stoffe als Funktion der Konzentration. *Kolloid-Zeitschrift* **97** (3), 313–321.
- EINSTEIN, A. 1906 Eine neue Bestimmung der Moleküldimensionen. *Ann. Phys.* **324** (2), 289–306.
- EINSTEIN, A. 1911 Berichtigung zu meiner Arbeit: Eine neue Bestimmung der Moleküldimensionen. *Ann. Phys.* **339** (3), 591–592.
- EVANS, K. E., NAKANSAH, M. A., HUTCHINSON, I. J. & ROGERS, S. C. 1991 Molecular network design. *Nature* **353**, 124.
- FRANKEL, N. A. & ACRIVOS, A. 1967 On the viscosity of a concentrated suspension of solid spheres. *Chem. Eng. Sci.* **22** (6), 847–853.
- FREUND, J. B. 2013 The flow of red blood cells through a narrow spleen-like slit. *Phys. Fluids* **25** (11), 110807.
- FRIJTERS, S., GÜNTHER, F. & HARTING, J. 2012 Effects of nanoparticles and surfactant on droplets in shear flow. *Soft Matter* **8** (24), 6542–6556.
- GALLIER, S., LEMAIRE, E., LOBRY, L. & PETERS, F. 2016 Effect of confinement in wall-bounded non-colloidal suspensions. *J. Fluid Mech.* **799**, 100–127.
- GALLIER, S., LEMAIRE, E., PETERS, F. & LOBRY, L. 2014 Rheology of sheared suspensions of rough frictional particles. *J. Fluid Mech.* **757**, 514–549.
- GLOWINSKI, R., PAN, T.-W., HESLA, T., JOSEPH, D. D. & PERIAUX, J. 2001 A fictitious domain approach to the direct numerical simulation of incompressible viscous flow past moving rigid bodies: application to particulate flow. *J. Comp. Phys.* **169** (2), 363–426.
- GROSS, M., KRÜGER, T. & VARNIK, F. 2014 Rheology of dense suspensions of elastic capsules: normal stresses, yield stress, jamming and confinement effects. *Soft matter* **10** (24), 4360–4372.
- GUAZZELLI, E. & POULIQUEN, O. 2018 Rheology of dense granular suspensions. *J. Fluid Mech.* **852**, P1.
- HÄNER, E., HEIL, M. & JUEL, A. 2020 Deformation and sorting of capsules in a T-junction. *J. Fluid Mech.* **885**.
- HARDEMAN, M. R., GOEDHART, P. T., DOBBE, J. G. G. & LETTINGA, K. P. 1994 Laser-assisted optical rotational cell analyser (LORCA); I. A new instrument for measurement of various structural hemorheological parameters. *Clin. Hem.* **14** (4), 605–618.

- HECHT, M. & HARTING, J. 2010 Implementation of on-site velocity boundary conditions for D3Q19 lattice Boltzmann simulations. *J. of Statistical Mechanics: Theory and Experiment* **2010** (01), P01018.
- KAOU, B., JONK, R. & HARTING, J. 2014 Interplay between microdynamics and macrorheology in vesicle suspensions. *Soft Matter* **10** (26), 4735–4742.
- KRIEGER, I. M. & DOUGHERTY, T. J. 1959 A mechanism for non-Newtonian flow in suspensions of rigid spheres. *Transactions of the Society of Rheology* **3** (1), 137–152.
- KRÜGER, T. 2012 *Computer simulation study of collective phenomena in dense suspensions of red blood cells under shear*. Springer Science & Business Media.
- KRÜGER, T., FRIJTERS, S., GÜNTHER, F., KAOU, B. & HARTING, J. 2013 Numerical simulations of complex fluid-fluid interface dynamics. *Eur. Phys. J. ST* **222** (1), 177–198.
- KRÜGER, T., KAOU, B. & HARTING, J. 2014 Interplay of inertia and deformability on rheological properties of a suspension of capsules. *J. Fluid Mech.* **751**, 725–745.
- KRÜGER, T., VARNIK, F. & RAABE, D. 2011 Efficient and accurate simulations of deformable particles immersed in a fluid using a combined immersed boundary lattice Boltzmann finite element method. *Comput. Math. Appl.* **61** (12), 3485–3505.
- LAC, E., BARTHÈS-BIESEL, D., PELEKASIS, N. A. & TSAMOPOULOS, J. 2004 Spherical capsules in three-dimensional unbounded Stokes flows: effect of the membrane constitutive law and onset of buckling. *J. Fluid Mech.* **516**, 303–334.
- LE, D. V. 2010 Effect of bending stiffness on the deformation of liquid capsules enclosed by thin shells in shear flow. *Phys. Rev. E* **82** (1), 016318.
- LÉVY, M.-C. & EDWARDS-LÉVY, F. 1996 Coating alginate beads with cross-linked biopolymers: A novel method based on a transacylation reaction. *J. Microencapsul.* **13** (2), 169–183.
- LI, X. & SARKAR, K. 2008 Front tracking simulation of deformation and buckling instability of a liquid capsule enclosed by an elastic membrane. *J. Comp. Phys.* **227** (10), 4998–5018.
- LI, X. Z., BARTHÈS-BIESEL, D. & HELMY, A. 1988 Large deformations and burst of a capsule freely suspended in an elongational flow. *J. Fluid Mech.* **187**, 179–196.
- LOEWENBERG, M. & HINCH, E. J. 1996 Numerical simulation of a concentrated emulsion in shear flow. *J. Fluid Mech.* **321**, 395–419.
- MARON, S. H. & PIERCE, P. E. 1956 Application of Ree-Eyring generalized flow theory to suspensions of spherical particles. *J. of Colloid Science* **11** (1), 80–95.
- MATSUNAGA, D., IMAI, Y., YAMAGUCHI, T. & ISHIKAWA, T. 2016 Rheology of a dense suspension of spherical capsules under simple shear flow. *J. Fluid Mech.* **786**, 110–127.
- MITTAL, R. & IACCARINO, G. 2005 Immersed boundary methods. *Ann. Rev. Fluid Mech.* **37**, 239–261.
- MIYAZAWA, K., YAJIMA, I., KANEDA, I. & YANAKI, T. 2000 Preparation of a new soft capsule for cosmetics. *J. Cosmet. Sci.* **51** (4), 239–252.
- MOONEY, M. 1951 The viscosity of a concentrated suspension of spherical particles. *J. Colloid Sci.* **6** (2), 162–170.
- MUELLER, S., LLEWELLIN, E. W. & MADER, H. M. 2010 The rheology of suspensions of solid particles. In *P. R. Soc. A*, , vol. 466, pp. 1201–1228. The Royal Society.
- MUNARIN, F., PETRINI, P., FARE, S. & TANZI, M. C. 2010 Structural properties of polysaccharide-based microcapsules for soft tissue regeneration. *J. Mater. Sci. Mater. Med.* **21** (1), 365–375.
- NEUBAUER, M. P., POEHLMANN, M. & FERY, A. 2014 Microcapsule mechanics: From stability to function. *Adv. Colloid Interface Sci.* **207**, 65–80.
- PESKIN, C. S. 2002 The immersed boundary method. *Acta numerica* **11**, 479–517.
- RAMANUJAN, S. & POZRIKIDIS, C. 1998 Deformation of liquid capsules enclosed by elastic membranes in simple shear flow: large deformations and the effect of fluid viscosities. *J. Fluid Mech.* **361**, 117–143.
- ROSTI, M. E., BRANDT, L. & MITRA, D. 2018 Rheology of suspensions of viscoelastic spheres: Deformability as an effective volume fraction. *Phys. Rev. Fluids* **3** (1), 012301.
- SAGIS, L. M. C., DE RUITER, R., MIRANDA, F. J. R., DE RUITER, J., SCHROËN, K., VAN AELST, A. C., KIEFT, H., BOOM, R. & VAN DER LINDEN, E. 2008 Polymer microcapsules with a fiber-reinforced nanocomposite shell. *Langmuir* **24** (5), 1608–1612.
- SARI, A., ALKAN, C. & KARAIPEKLI, A. 2010 Preparation, characterization and thermal

- properties of PMMA/n-heptadecane microcapsules as novel solid-liquid microPCM for thermal energy storage. *Appl. Energ.* **87** (5), 1529–1534.
- SIEROU, A. & BRADY, J. F. 2002 Rheology and microstructure in concentrated noncolloidal suspensions. *J. Rheol.* **46** (5), 1031–1056.
- SINHA, K. & GRAHAM, M. D. 2015 Dynamics of a single red blood cell in simple shear flow. *Phys. Rev. E* **92** (4), 042710.
- SKALAK, R. 1973 Modelling the mechanical behavior of red blood cells. *Biorheology* **10** (2), 229–238.
- SKALAK, R., TOZEREN, A., ZARDA, R. P. & CHIEN, S. 1973 Strain energy function of red blood cell membranes. *Biophys. J.* **13** (3), 245–264.
- STICKEL, J. J. & POWELL, R. L. 2005 Fluid mechanics and rheology of dense suspensions. *Ann. Rev. Fluid Mech.* **37**, 129–149.
- SURYANARAYANA, C., RAO, K. C. & KUMAR, D. 2008 Preparation and characterization of microcapsules containing linseed oil and its use in self-healing coatings. *Prog. Org. Coat.* **63** (1), 72–78.
- TAYLOR, G. I. 1934 The formation of emulsions in definable fields of flow. *P. R. Soc. A* **146** (858), 501–523.
- VLAHOVSKA, P. M. & GRACIA, R. S. 2007 Dynamics of a viscous vesicle in linear flows. *Phys. Rev. E* **75** (1), 016313.
- WALTER, A., REHAGE, H. & LEONHARD, H. 2001 Shear induced deformation of microcapsules: shape oscillations and membrane folding. *Colloids Surf. A Physicochem. Eng. Asp.* **183**, 123–132.
- WOUTERS, M. P. J., AOUANE, O., KRÜGER, T. & HARTING, J. 2019 Mesoscale simulation of soft particles with tunable contact angle in multi-component fluids. *Phys. Rev. E* **100**, 033309.
- ZHAO, H. & SHAQFEH, E. S. G. 2013 The dynamics of a non-dilute vesicle suspension in a simple shear flow. *J. Fluid Mech.* **725**, 709–731.